Time-dependent calculations of electron energy distribution functions for neon gas in the presence of intense XFEL radiation

2013 J. Phys. B: At. Mol. Opt. Phys. 46 235004

(http://iopscience.iop.org/0953-4075/46/23/235004)

OPEN ACCESS
IOP Publishing
Journal of Physics B: Atomic, Molecular and Optical Physics

J. Phys. B: At. Mol. Opt. Phys. **46** (2013) 235004 (8pp)
doi:10.1088/0953-4075/46/23/235004

Time-dependent calculations of electron energy distribution functions for neon gas in the presence of intense XFEL radiation

J Abdallah Jr[1], **J Colgan**[1] **and N Rohringer**[2,3]

[1] Theoretical Division, Los Alamos National Laboratory, Los Alamos, NM 87545, USA
[2] Max Planck Institute for the Physics of Complex Systems, D-01187 Dresden, Germany
[3] Center for Free-Electron Laser Science, D-22607 Hamburg, Germany

E-mail: abd@lanl.gov

Received 27 August 2013, in final form 23 October 2013
Published 22 November 2013
Online at stacks.iop.org/JPhysB/46/235004

Abstract

Boltzmann electron kinetic simulations are performed to study the time development of the electron energy distribution function (EEDF) in plasma resulting from neon gas subject to a 40 fs x-ray free electron laser radiation source. The simulations are performed without any assumptions of electron temperature. The distributions are calculated as a function of time through 40 fs using Boltzmann kinetics, including the appropriate processes that alter state populations and electron energy. The calculations are also extended into the picosecond regime, after the laser pulse, to track the thermalization of free electrons. Results are presented that predict the evolution of the charge-state distribution, effective temperature, the photon spectrum, as well as the EEDF.

(Some figures may appear in colour only in the online journal)

1. Introduction

There have been many interesting applications [1–3] of x-ray free electron laser (XFEL) technology involving quasi-monochromatic high-energy laser photons interacting with matter. There have also been interesting applications of XFEL interactions with dense matter [4, 5]. The XFEL produces a monochromatic x-ray source at tunable wavelengths. The important process at high enough photon energies is the photo-ionization of inner shell electrons followed by fast auto-ionization [6–9]. Production of hollow atoms, having no electrons in the 1s shell, are also possible under XFEL conditions [10–12]. This involves consecutive photo-ionization of both K-shell electrons. Hollow atoms have also been observed in recent experiments using more conventional high intensity lasers [13]. The XFEL creates low-energy electrons from direct ionization of inner shell electrons and high-energy electrons from direct ionization of outer (less bound) electrons and auto-ionization of levels with inner shell vacancies. The free electrons form a time-dependent plasma which is characterized by the electron energy distribution function (EEDF). The EEDF for XFEL produced plasmas are not well known and a effective temperature based on energetics is generally assumed in XFEL modeling calculations [14].

The purpose of this paper is to simulate the EEDF for the plasma created when neon gas is irradiated by a realistic XFEL pulse, and to provide insight about the important processes occurring in the plasma under these conditions. The Boltzmann equations have been previously applied to the expansion of noble-gas clusters interacting with soft XFEL radiation [15, 16]. Unfortunately, there are no measurements of the EEDF for comparison purposes. The authors are unaware of any similar calculations under these conditions. Radiative properties of plasmas can be very sensitive [17–19] to the EEDF.

The approach used here is similar to previous calculations [20] used to model the EEDF resulting from the interaction of several hundred eV black-body radiation with cold argon gas. The EEDF is propagated in time by simultaneous solution of atomic rate equations and

Boltzmann electron kinetics using both electron and photon processes. The atomic kinetics keeps track of atomic state populations while the electron kinetics keeps track of the distribution of energy for free electrons. Electron-impact collisional excitation, de-excitation, ionization, electron–electron collisions, photo-excitation, de-excitation, photo-ionization, radiative recombination, auto-ionization, di-electronic capture and free–free absorption and emission were used in the kinetics.

The method used is briefly reviewed in section 2, the results of the simulations are discussed in section 3 and conclusions are presented in section 4.

2. Method

The method used for the present calculations has been described previously [20–23]. The black-body radiation field of [20] is replaced by a typical XFEL pulse. The XFEL pulse is approximated by a flat-top distribution function of a specified width for the entire duration of the pulse. Although XFELs based on the principle of self-amplified spontaneous emission (SASE) typically have a spiky, intrinsically incoherent temporal and spectral pulse profile, the overall charge-state distribution was demonstrated to be rather independent of the temporal coherence properties of the XFEL [7]. It will hence be a good approximation to determine the EEDF for an averaged, flat-top temporal pulse profile, rather than to perform the ensemble average over many SASE XFEL realizations. Parameter values were chosen to approximate experimental conditions [2]. The EEDF is calculated using this procedure for the duration of the pulse. In addition, calculations are performed after the pulse duration to study electron thermalization. Radiation and heat transport effects and hydrodynamic expansion were not included.

The atomic data used in the simulations were generated using the Los Alamos suite of atomic physics codes. The CATS code [24], which is an adaptation of Cowan's atomic structure codes [25], was used to calculate wavefunctions, energy levels, oscillator strengths, and plane-wave Born collision strengths within the configuration-average approximation. Electron-impact ionization, photo-ionization and auto-ionization cross sections were calculated using the multi-purpose ionization GIPPER code [26, 27]. The latter two processes were calculated explicitly with distorted-wave continuum functions while the electron-impact ionization calculations used scaled hydrogenic cross sections that were designed to reproduce distorted-wave calculations. Radiative, and di-electronic recombination rate coefficients were obtained from detailed balance. Three-body recombination is not important at the density considered here and was not included in these calculations to improve computational speed.

The configurations included in the calculations were as follows. For Ne-like through Li-like Ne, configurations of the type $[\mathrm{He}](2l)^{w}$, $[\mathrm{He}](2l)^{w-1}(3-5l')^{1}$, $(1\mathrm{s})^{1}(2l)^{w}(3-5l')^{1}$, $(1\mathrm{s})^{1}(2l)^{w-1}(3l')^{2}$, $(1\mathrm{s})^{1}(2l)^{w-1}(3l')^{1}(4-5l'')^{1}$, $(1\mathrm{s})^{0}(2l)^{w}(3l')^{2}$, and $(1\mathrm{s})^{0}(2l)^{w}(3l')^{1}(4-5l'')^{1}$ were included. The restrictions $l', l'' = 0-3$ are imposed. Here w ranges from 8 for Ne-like Ne to 1 for Li-like Ne. For He-like Ne configurations of the type $(1\mathrm{s})^{2}$, $(1\mathrm{s})^{1}(2-7l)^{1}$ and $(1\mathrm{s})^{0}(2-5l')^{2}$ were included, where now $l = 0-6$ (as applicable) and $l' = 0-3$. The notation [He] corresponds to the He-like ground-state core $1\mathrm{s}^{2}$. For H-like Ne all configurations of the type $(1-7l)^{1}$ were included (with $l = 0-6$ as applicable). This model generated around 2000 configurations for all Ne ionization stages. Note that hollow atom type configurations are used in the atomic model. The configuration-average atomic model was used for all calculations performed in this paper.

The Los Alamos atomic kinetics and opacity code ATOMIC [28] was used to perform the EEDF calculations. In the present case we start out with cold neutral neon gas, with atom number density 1.6×10^{19} cm^{-3}. This corresponds to a gas pressure of about 500 torr. The time-dependent kinetics integration time span is divided into time intervals. In total, 40 time intervals were chosen to accurately describe the EEDF during the XFEL pulse. The pulse photon energy was centered around 1070 eV, with a width of 10 eV, and a duration of 40 fs. Laser intensities of 2×10^{17} and 10^{18} W cm^{-3} were used. The EEDF was carefully chosen to consist of 900 equally spaced electron energy bins between 0 and 1800 eV. This bin size (2 eV) was determined by performing calculations by increasing the number of bins until the resulting EEDF converged. All the atoms were assumed initially to be in the ground-state of neutral neon. The initial level populations are held constant during the first interval to propagate the EEDF from the beginning to the end of the interval. Then the calculated EEDF is used to propagate the initial level populations based on atomic kinetics to the end of the interval. The procedure is repeated over all intervals for the entire time span of interest. Note that the only input to the model is the initial conditions, the atomic data and the radiation field. Also note that all times specified in this paper are referenced with respect to the beginning of the laser pulse.

3. Results and discussion

Figure 1 shows the calculated charge-state distribution during the 40 fs XFEL laser pulse of 2×10^{17} W cm^{-3} using the full model described in the previous section. It shows the evolution of ionization from neutral neon to 40 fs where the dominant charge state is Ne^{+6} and the mean ion charge is 6.43. Note that the ionization rate decreases rapidly by about 15 fs, because the K-shell binding energy of Ne^{+6} and higher charge states exceeds the laser energy of 1070 eV. Note that Ne^{+1} never becomes dominant. This is because the main ionization channel from neutral neon is K-shell photo-ionization while auto-ionization is the main channel from the singly ionized species. Ne^{+1} is a conduit for ionization to Ne^{+2}. It is clear that the auto-ionization rate from the singly charged ion with a K-shell hole exceeds the neutral photo-ionization rate at this laser intensity. This sequence of photo-ionization followed by auto-ionization again produces a large population of doubly charged ions and a small population of triply charged ions, as also experimentally observed [6] and previously predicted [7]. Note that the strong population difference between odd and

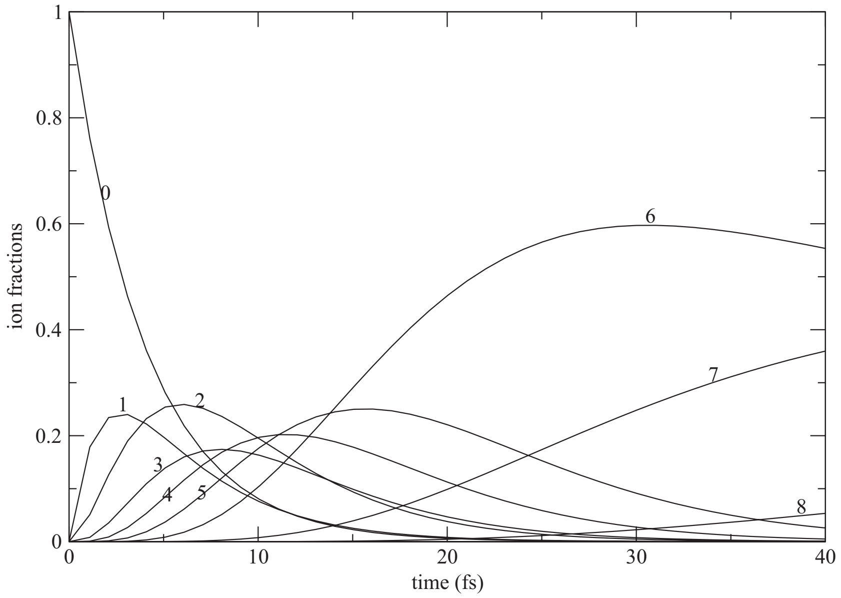

Figure 1. The calculated charge-state distribution (unitless) as a function of time (fs) for a 40 fs, 2 × 10^{17} W cm^{-3} XFEL laser pulse. Each curve is labeled by its corresponding ion charge, thus 0 is neutral neon, 1 is singly charged neon, etc.

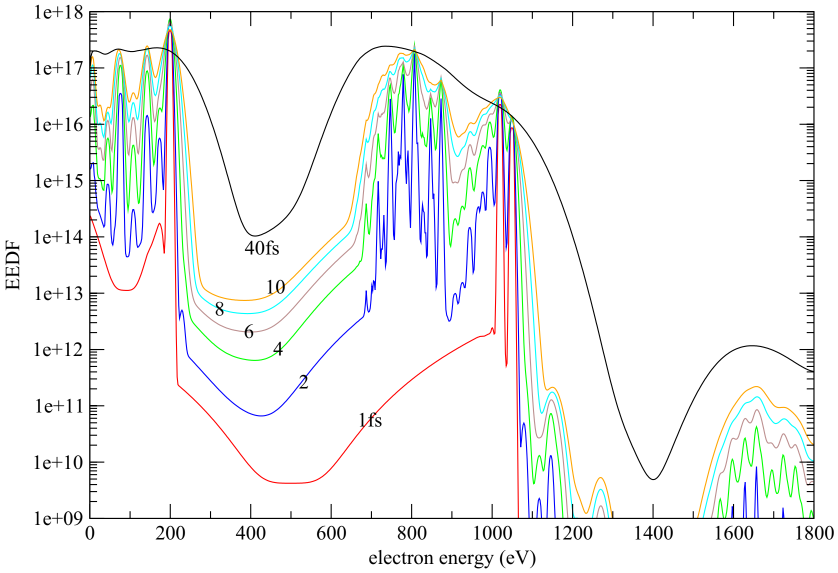

Figure 2. The calculated electron energy distribution function (EEDF) in cm^{-3} eV^{-1} as a function of electron energy (eV) for various times during irradiation by a 40 fs, 2 × 10^{17} W cm^{-3} XFEL laser pulse. Each curve is labeled by its corresponding time (fs).

even charge states estimated in our theory might be slightly over-emphasized. It was recently shown [29] that shake-up and shake-off processes accompanying photo-ionization, which are not included in the current treatment, tend to decrease the difference in populations of even and odd charge states.

Figure 2 shows the calculated EEDF for the case corresponding to figure 1. The prominent feature at early time (about 1 fs) is the bump at 200 eV which results from the direct photo-ionization of the K shell of neutral neon. The K shell is ionized preferentially over the L-shell because the XFEL photon energy lies close to the K-shell threshold resulting in a larger cross section. The bump is located at 200 eV because the K shell ionization energy is approximately 870 eV, therefore the ionized electron has a energy of 1070−870 eV = 200 eV. Additional features with energy between 1000 and 1100 eV correspond to photo-ionization of the 2s and 2p valence electrons. These energies correspond roughly to 1070−50 eV = 1020 eV and 1070 −20 eV = 1050 eV where 50 eV is the binding energy of a 2s electron and 20 eV is the binding energy of the 2p electron. The 2s bump in the EEDF is larger than the 2p bump because its cross section is larger at a photon energy of 1070 eV.

At energies below 200 eV and times greater than 1 fs, features in the electron spectrum appear that correspond to photo-electrons produced by K-shell ionization from higher stages of ionization. Here the ion charge increases with decreasing electron energy. Each distinct bump corresponds essentially to a different stage of ionization. Note that the features corresponding to Ne^{0}, Ne^{+2}, Ne^{+4} and Ne^{+6} are more intense than those of Ne^{+1}, Ne^{+3} and Ne^{+5}. This is due to the

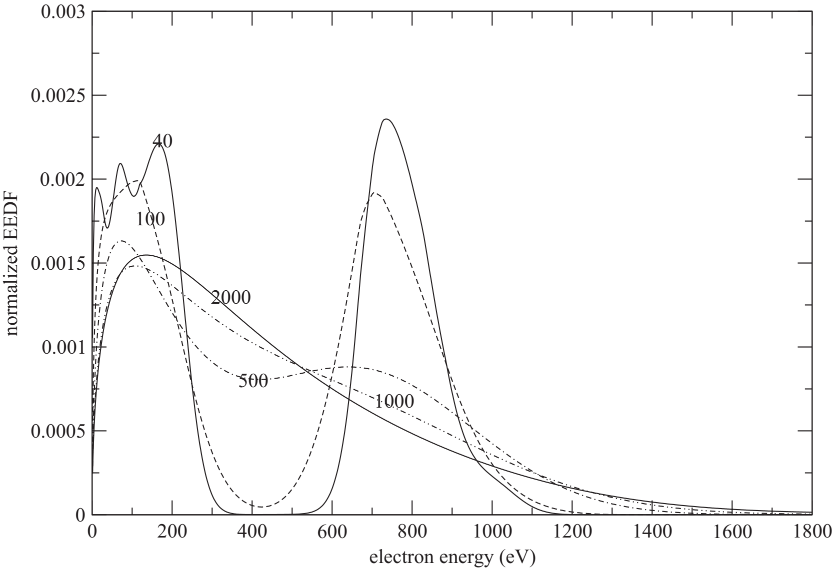

Figure 3. The calculated normalized electron energy distribution function (EEDF) in eV^{-1} as a function of electron energy (eV) for various times after irradiation by a 40 fs, 2×10^{17} W cm^{-3} XFEL laser pulse. Each curve is labeled by its corresponding time (fs).

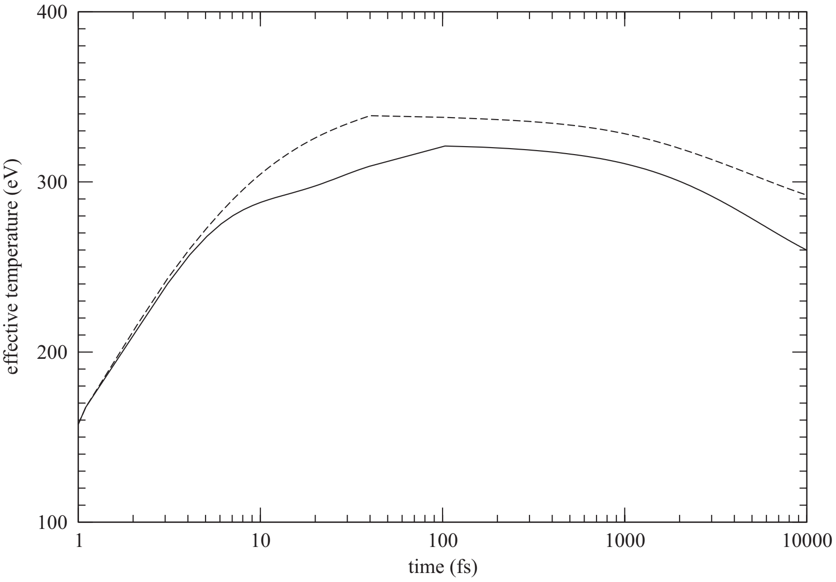

Figure 4. The calculated effective temperature (kT^*) in eV as a function of time (fs) for during and after irradiation by 40 fs XFEL laser pulses. The solid line corresponds to an intensity of 2×10^{17} W cm^{-3} and the dashed line corresponds to a intensity of 1×10^{18} W cm^{-3}.

photo-ionization–auto-ionization sequence discussed above. The ion stages which are driven by photo-ionization have large signatures in this region.

The EEDF shows various high-energy features above 700 eV. The spectrum of ejected Auger electrons occurs at energies between 700 and 900 eV. The largest feature near 800 eV corresponds to the $1s^12s^22p^6 - 1s^22s^22p^4$ auto-ionizing transition. The feature near 875 eV actually corresponds to the Auger decay of the hollow atom $1s^02s^22p^6$ state. Between 900 and 1100 eV, electrons are produced by photo-ionization of valence electrons from various charge states.

It is interesting to note that small features also occur beyond about 1100 eV. At first glance, this result may seem peculiar because electrons are being produced with energies exceeding the XFEL photon energy. These are mainly produced by electron collisions with atoms (ions). An electron collides with an atom (ion) in an excited state, the atom (ion) de-excites to a lower state and the scattering electron gains the energy difference. The features have structure because the EEDF has structure. Note that this effect is orders of magnitude smaller than photo-ionization and auto-ionization.

Note that as time increases to 40 fs many of the distinct features are washed out by the electron–electron interactions. At 40 fs a low-energy component to the EEDF with some structure is left below 200 eV. There is a valley with few electrons from 200 to 600 eV. Between 600 and 1200 eV there is a large asymmetric tail of hot electrons and a smaller one beyond 1400 eV.

It is also interesting to follow the EEDF after the laser is turned off. Figure 3 shows the predicted EEDF at various times (fs) from the beginning of the laser pulse. The curve labeled at 40 fs occurs at the end of the laser pulse and has

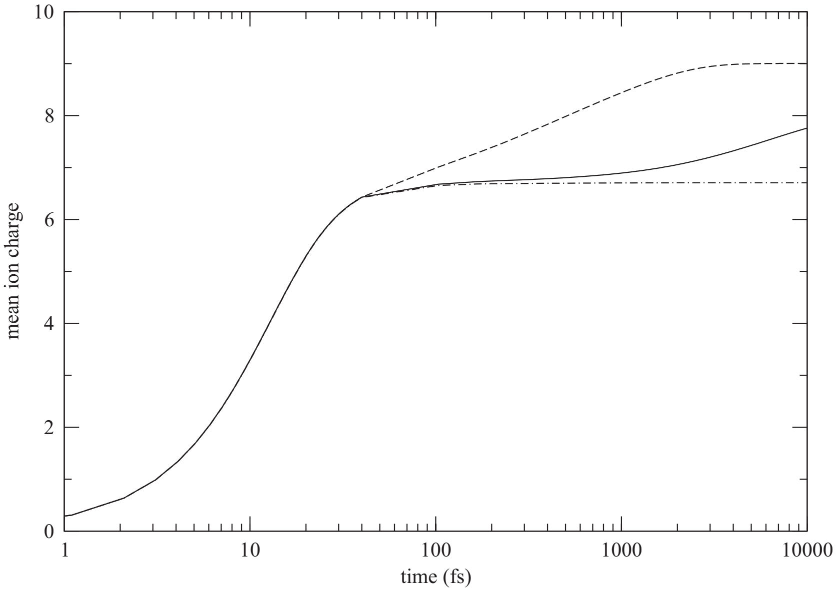

Figure 5. The calculated mean ion charge (Z^*) as a function of time (fs) during and after irradiation by a 40 fs 2×10^{17} W cm^{-3} XFEL laser pulse. The solid line is the result of the full Boltzmann model, the dashed line is the result of using the Maxwellian model with effective temperatures, and the dash–dotted line is the full model neglecting electron–atom (ion) collisions.

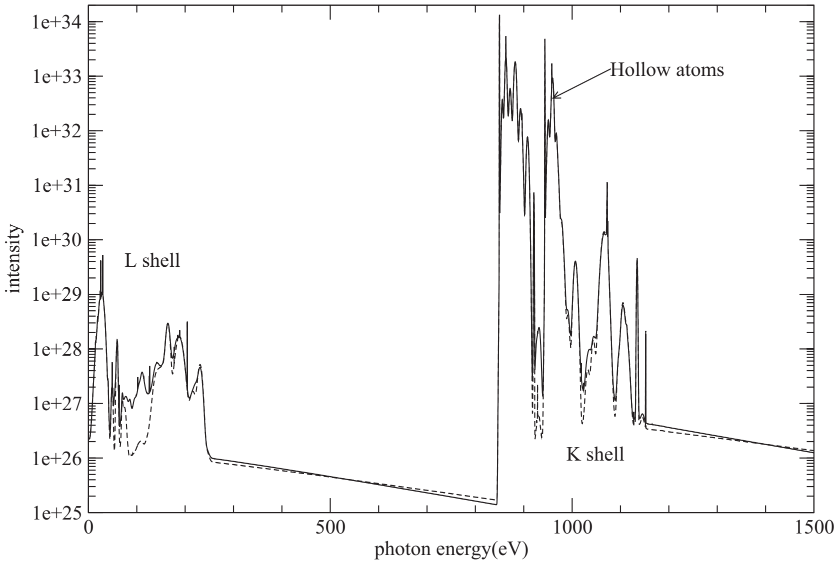

Figure 6. The calculated photon emission spectrum in eV cm^{-3}sec^{-1} per unit energy interval (eV) as a function of photon energy in eV at 10 fs into a 40 fs 2×10^{17} W cm^{-3} XFEL laser pulse. The solid line is computed using populations from the full Boltzmann model and the dashed line from populations of the same model neglecting electron–atom (ion) collisions.

been discussed above. Note that a linear scale is used here and the curves have been normalized by dividing out the electron density. Note that as time increases both the high-energy tail and the low-energy component deplete to fill in the valley. The high-energy tail depletes faster than low-energy component. The EEDF takes on a bi-modal form very quickly. However, the high-energy tail is still noticeable even at 1000 fs, or 1 ps. The distribution thermalizes to essentially Maxwellian form by 2000 fs (2 ps).

It is also informative to calculate the effective temperature as a function of time. This temperature corresponds to a Maxwellian distribution having the equivalent mean kinetic energy as the calculated EEDF [20]. The solid line in figure 4 shows the effective temperature as a function of time for this case. The effective temperature increases rapidly until about 10fs, where it slows down as it approaches the Ne^{+6} barrier. This temperature continues to grow until 100 fs, where it plateaus and then cools. Note that it grows even after the XFEL is turned off at 40 fs, which is due to decay of the remaining core excited states by Auger and radiative processes.

It is also interesting to use Maxwellian distributions with the effective temperatures shown in figure 4 to represent the electrons in the modeling calculations for comparison purposes. Figure 5 shows the calculated average charge state using effective temperatures (dashed line) compared to the full Boltzmann model (solid line) and the Boltzmann model neglecting electron–atom (ion) collisions. Note that during the 40fs laser pulse all the models agree. This is not surprising

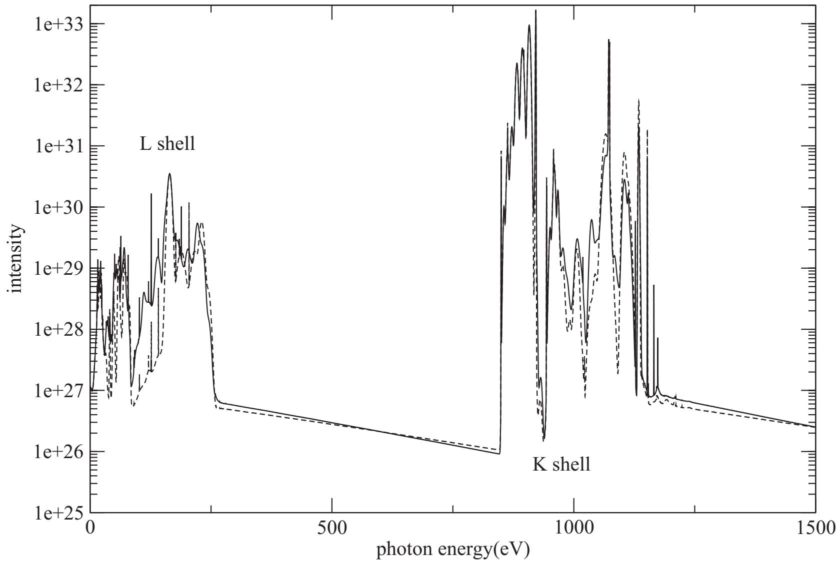

Figure 7. The calculated photon emission spectrum in eV $\mathrm{cm}^{-3}\mathrm{sec}^{-1}$ per unit energy interval (eV) as a function of photon energy in eV at the end of a 40 fs 2×10^{17} W cm^{-3} XFEL laser pulse. The solid line is computed using populations from the full Boltzmann model and the dashed line from populations of the same model neglecting electron–atom (ion) collisions.

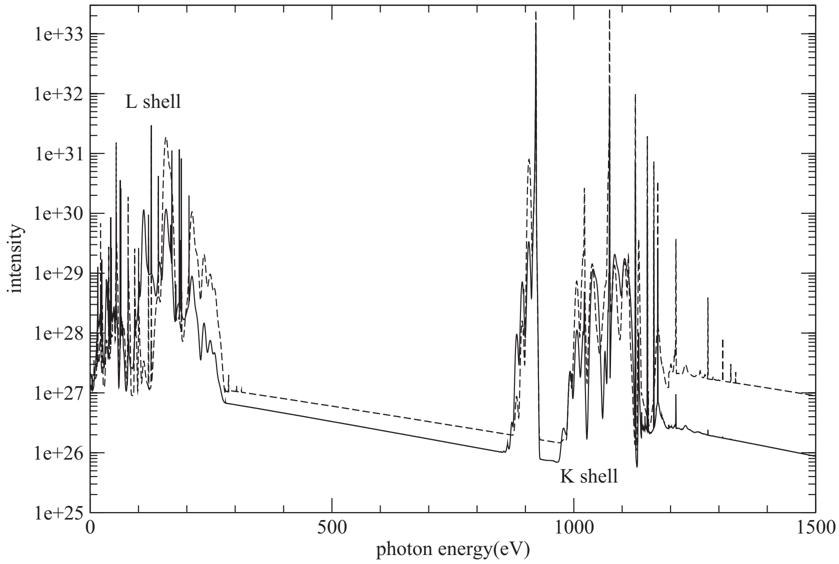

Figure 8. The calculated photon emission spectrum in eV $\mathrm{cm}^{-3}\mathrm{sec}^{-1}$ per unit energy interval (eV) as a function of photon energy in eV at 500 fs after a 40 fs 2×10^{17} W cm^{-3} XFEL laser pulse is turned on. The solid line is computed using populations from the full Boltzmann model and the dashed line from populations from the Maxwellian model using effective temperatures.

since photon processes dominate electron processes during a laser pulse of this intensity. After the XFEL pulse, the electron processes dominate. The Maxwellian model predicts more ionization than the Boltzmann models after the laser pulse. This is because the hot electrons resulting from the Boltzmann EEDF (see figure 3) are less efficient for ionizing valence electrons than the thermal electrons of the Maxwellian distribution. Note the increased ionization of the full Boltzmann model as more hot electrons are converted into thermal electrons at later times. As expected, the Boltzmann model without electron–atom (ion) collisions flattens out because further ionization is not possible.

The photon emission spectra as a function of time can be calculated using the populations derived by the various kinetic models. For simplicity, the spectra calculated here are based on configuration-average populations using unresolved transition arrays [30]. Note that all the spectra shown correspond to snapshots using the populations calculated at the specified time. During the laser pulse both the Boltzmann model and the effective Maxwellian model give nearly identical spectra. This is because the XFEL radiation is the dominating factor for populating levels and there are enough low-energy electrons in both distributions to collisionally mix the upper levels to the same population distribution. This is illustrated in figure 6. The spectral features in figure 6 correspond to L-shell transitions, below 300 eV, a band of transitions involving single K-shell 2p − 1s transitions from 800 to 900 eV, a band of hollow atom transitions from 900 to 1000 eV, plus some higher energy transitions. Figure 6 shows the calculated spectrum at 10 fs using the full Boltzmann model

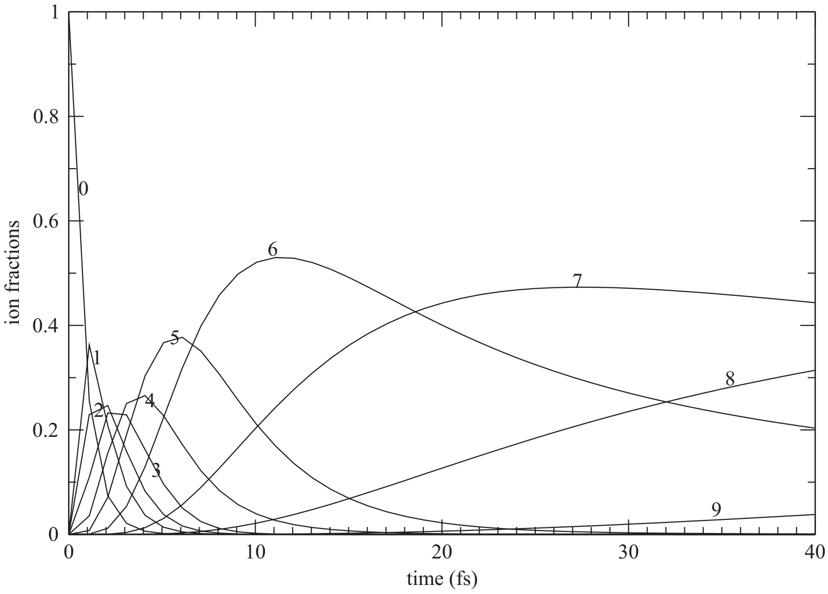

Figure 9. The calculated charge-state distribution (unitless) as a function of time (fs) for a 40 fs, 1 × 10^{18} W cm^{-3} XFEL laser pulse. Each curve is labeled by its corresponding ion charge, thus 0 is neutral neon, 1 is singly charged neon, etc.

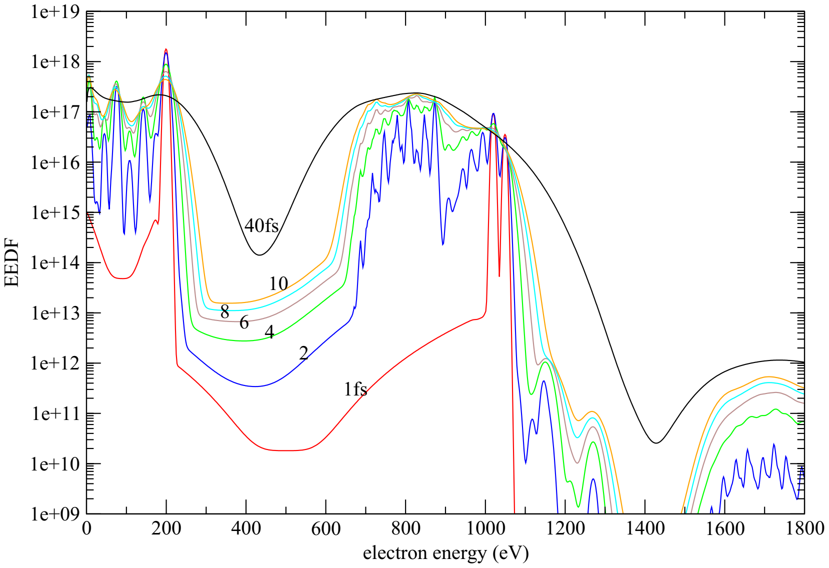

Figure 10. The calculated electron energy distribution function (EEDF) in $\mathrm{cm}^{-3}\mathrm{eV}^{-1}$ as a function of electron energy (eV) for various times during irradiation by a 40 fs, 1 × 10^{18} W cm^{-3} XFEL laser pulse. Each curve is labeled by its corresponding time (fs).

(solid line). The model using the effective temperatures shown in figure 4 yields an essentially identical spectrum (not shown) to the full Boltzmann model for the reasons discussed above. Calculations based on the same model neglecting electron–atom excitation and ionization were included (dashed line) to assess the role of such collisions during the laser pulse. In general, the spectrum is not affected by electron–atom collisions except near 100 eV in the L-shell. It is interesting to note that the lines in the K-shell region alternate in intensity, each peak being emission from a different ion stage. This is also a consequence of the photo-ionization–auto-ionization mechanism discussed above, and corresponds to the possibility of emission when the K-shell vacancy is created by the laser. Figure 7 shows the same comparison at 40 fs at the end of the laser pulse. Here the electron–atom collisions play a more important role for both the L-shell features and the K-shell features. Note that the L-shell features have increased in intensity due to increased electron density. Also note that the hollow atom lines have decreased in intensity relative to the single vacancy transitions compared to the 10 fs calculation (figure 6). The alternating intensities are not apparent for the higher charged ions in figure 7.

Figure 8 shows a calculated spectrum at 500 fs, 460 fs after the pulse has been turned off. In this figure the dashed line is calculated as a Maxwellian with an effective temperature shown in figure 4. Note there is a large difference in the two spectra as one might expect from the difference in the degree of ionization shown in figure 5. This means that the spectrum is sensitive to the EEDF after the laser is turned off. Also note that the K-shell emission has decreased significantly compared to figures 6 and 7, and that the band of hollow atom transitions has disappeared.

Figure 9 shows the calculated charge-state distribution using the full Boltzmann model for the same conditions as figure 1 except the XFEL intensity has been increased to 1×10^{18} W cm^{-3}, that is, five times more intense than the previously studied case. Note that at early times the radiation field is strong enough to more quickly ionize through neutral neon so that the ion stages ionize sequentially. Ions Ne^{+6} and Ne^{+7} are more difficult to ionize because their binding energy exceeds 1070 eV. Most of Ne^{+6} is formed by auto-ionization of Ne^{+5}, while Ne^{+7} is formed slowly by electron collisions. Figure 4 shows a comparison of the effective electron temperatures calculated at both intensities. In this case the plasma is predicted to cool immediately after the pulse at 40 fs. This is because the Ne^{+6} population is depleted. Figure 9 shows the calculated EEDF for this case. Note that figure 10 has features similar to figure 2. Also, the structure in the EEDF is washed out at earlier times than the 2×10^{17} W cm^{-3} case because of increased ionization.

4. Conclusions

Model calculations have been performed to calculate the time-dependent electron energy distribution function and ionization state for a cold neon gas in the presence of nominal x-ray free electron laser radiation field of intensity 2×10^{17} W cm^{-3}. The results show that the electron energy distribution function (EEDF) are highly non-Maxwellian at the end of the laser pulse. The EEDF shows structure at early times due to K-shell and L-shell photo-ionization, auto-ionization and electron-ion de-excitation. The main process of direct photo-ionization of K-shell electrons followed by auto-ionization is evident in the calculated EEDF and calculated photon spectra. A Maxwellian distribution defined with an effective temperature is adequate for modeling calculations during the pulse, when photon processes dominate. A non-Maxwellian distribution of electrons is predicted for several picoseconds after the pulse. This EEDF produces less ionization and a different photon spectrum than the effective temperature model. Calculations show strong emission from hollow atom states early in the pulse which decrease during the pulse and disappear after the pulse. EEDF calculations were also performed for an increased intensity of 1×10^{18} W cm^{-3}. For these calculations, the EEDF features wash out at earlier times due to increased electron density.

Acknowledgments

The Los Alamos National Laboratory is operated by Los Alamos National Security, LLC for the National Nuclear Security Administration of the US Department of Energy under contract no. DE-AC5206NA25396.

References

[1] Rosmej F B, Lee R W and Schneider D H G 2007 *High Energy Density Phys.* **3** 218

[2] Rohringer N *et al* 2012 *Nature* **481** 488

[3] Vinko S M *et al* 2012 *Nature* **482** 56

[4] Rosmej F B 2012 *Free Electron Lasers* ed S Varro (Intech) pp 187–212

[5] Galtier E *et al* 2011 *Phys. Rev. Lett.* **106** 164801

[6] Young L *et al* 2010 *Nature* **466** 59

[7] Rohringer N and Santra R 2007 *Phys. Rev.* A **76** 033416

[8] Fukuzawa H *et al* 2013 *Phys. Rev. Lett.* **110** 173005

[9] Son S-K and Santra R 2012 *Phys. Rev.* A **85** 063415

[10] Tamasaku K *et al* 2013 *Phys. Rev. Lett.* **111** 043001

[11] Fang L *et al* 2010 *Phys. Rev. Lett.* **105** 083005

[12] Frasinski L J *et al* 2013 *Phys. Rev. Lett.* **111** 073002

[13] Colgan J *et al* 2013 *Phys. Rev. Lett.* **110** 125001

[14] Ciricosta O, Chung H-K, Lee R W and Wark J S 2011 *High Energy Density Phys.* **7** 111–6

[15] Ziaja B, de Castro A R B, Weckert E and Moeller T 2006 *Eur. Phys. J.* D **40** 465

[16] Ziaja B, Wabnitz H, Wang F, Weckert E and Moeller T 2009 *Phys. Rev. Lett.* **102** 205002

[17] Hansen S B and Shlyaptseva A S 2004 *14th Topical Conf. on Atomic Processes in Plasmas* ed J S Cohen, S Mazevet and D P Kilcrease (New York: AIP) pp 213–22

[18] Abdallah J Jr, Faenov A Ya, Pikuz T A, Wilke M D, Kyrala G A and Clark R E H 1999 *J. Quant. Spectrosc. Radiat. Transfer* **62** 1

[19] Abdallah J Jr, Faenov A Y, Hammer D, Pikuz S A, Csanak G and Clark R E H 1996 *Phys. Scr.* **53** 705

[20] Abdallah J Jr and Colgan J 2012 *J. Phys. B: At. Mol. Opt. Phys.* **45** 2

[21] Bretagne J, Godart J and Puech V 1982 *J. Phys. D: Appl. Phys.* **15** 2205

[22] Abdallah J Jr *et al* 2003 *Phys. Rev.* A **68** 063201

[23] Sherrill M E *et al* 2006 *Phys. Rev.* E **73** 066404

[24] Abdallah J, Clark R E H and Cowan R D 1988 *Los Alamos Manual No.* LA 11436-M-I (New Mexico: Los Alamos National Laboratory)

[25] Cowan R D 1981 *The Theory of Atomic Structure and Spectra* (Berkeley, CA: University of California Press)

[26] Archer B J, Clark R E H, Fontes C J and Zhang H L 2002 *Los Alamos Memorandum* LA-UR-02-1526

[27] Abdallah J Jr, Collins L A, Csanak G, Petschek A G and Schappert G T 1995 *Z. Phys.* D **34** 233

[28] Hakel P, Sherrill M E, Mazevet S, Abdallah J Jr, Colgan J, Kilcrease D P, Magee N H, Fontes C J and Zhang H L 2006 *J. Quant. Spectrosc. Radiat. Transfer* **99** 265

[29] Doumy G *et al* 2011 *Phys. Rev. Lett.* **106** 083002

[30] Bauche-Arnoult C, Bauche J and Klapish M 1979 *Phys. Rev.* A **20** 2424